Prediction of curvature ductility factor for FRP strengthened RHSC beams using ANFIS and regression models

H. Ebrahimpour Komleh and A.A. Maghsoudi[*]

Civil Engineering Department, Faculty of Engineering, Shahid Bahonar University of Kerman, Kerman, Iran

Abstract. Nowadays, fiber reinforced polymer (FRP) composites are widely used for rehabilitation, repair and strengthening of reinforced concrete (RC) structures. Also, recent advances in concrete technology have led to the production of high strength concrete, HSC. Such concrete due to its very high compression strength is less ductile; so in seismic areas, ductility is an important factor in design of HSC members (especially FRP strengthened members) under flexure. In this study, the Adaptive Neuro-Fuzzy Inference System (ANFIS) and multiple regression analysis are used to predict the curvature ductility factor of FRP strengthened reinforced HSC (RHSC) beams. Also, the effects of concrete strength, steel reinforcement ratio and externally reinforcement (FRP) stiffness on the complete moment-curvature behavior and the curvature ductility factor of the FRP strengthened RHSC beams are evaluated using the analytical approach. Results indicate that the predictions of ANFIS and multiple regression models for the curvature ductility factor are accurate to within -0.22% and 1.87% error for practical applications respectively. Finally, the effects of height to wide ratio (h/b) of the cross section on the proposed models are investigated.

Keywords: high strength concrete; FRP composites; multiple regression analysis; ANFIS; ductility

1. Introduction

Strengthening of reinforced concrete (RC) structures by fiber reinforced polymer (FRP) composites has become very popular around the world over the past decade due to the well-known advantages of FRP composites over conventional materials such as steel. Consequently, a great amount of research, both experimental and theoretical, has been conducted on the behavior of FRP-strengthened RC beams, slabs and columns (Foret and Limam 2008, Lignola *et al.* 2007, Teng *et al.* 2002).

One of the most common methods for flexural strengthening of RC beams with FRP materials is the externally bonded reinforcement (EBR) method. Main types of FRP composites used in EBR technique (in forms such as pultruded plates, fabrics, and sheets) are: carbon fiber reinforced polymers (CFRP), glass fiber reinforced polymers (GFRP). CFRP has a high strength and a high elastic modulus and is more expensive and its elongation at fracture is relatively small (1-1.5%),

---

*Corresponding author, Professor, E-mail: maghsoudi.a.a@uk.ac.ir

while GFRP is cheaper and has a relatively large elongation (3-5.4%). However, the elastic modulus of GFRP is significantly lower than that of CFRP. As a result, the ductility and stiffness of CFRP strengthened beams are noticeably lower and higher than those of GFRP strengthened beams (Xiong *et al.* 2004).

A vast number of failure mechanisms, upwards of 30 types according to some studies have been experimentally reported in RC beams strengthened with FRP sheets (Oehlers 2001). However, these can be generally classified into three main types of flexural, shear and debonding ruptures. Debonding mechanism is the most probable failure mode in FRP reinforced concrete beams. Such a failure is usually abrupt and uneconomical, and takes place by plate separation of the concrete surface before attaining the flexural capacity of the concrete beam (while neither of the concrete or FRP are damage separately). In such a case the structural member is unemployable anymore and results in incomplete exploitation of the reinforcing FRP plate. The most common type of abrupt debonding of FRP strips is the debonding of FRP strip together with the concrete substrate on the reinforcement steel, starting from one end or near one end and moving toward the center. Still, another type of abrupt debonding is the delamination of the FRP strip from the beam interface which starts from the strip end, removing with it a thin layer of the concrete. Debonding may also start in a flexural or a combined flexural-shear crack in a region far from the strip end and grow toward one end. A part of the concrete interface may also be sticking to the debonding strip in this case.

Various analytical methods are available to analyze beams strengthened with bonded FRP laminates. An analytical approach based on a cross-section analysis is easy and accurate to calculate the failure load of the strengthened beams. Also, this approach is applicable for design of the strengthened beams by FRP laminate (Teng *et al.* 2002). Malek *et al.* (1998), Rasheed *et al.* (2004), Chahrour and Soudki (2005), Toutanji *et al.* (2006), Akbarzadeh and Maghsoudi (2010) and Ebrahimpour and Maghsoudi (2013) presented analytical procedures based on the cross-section analysis to calculate the flexural strength of RC beams bonded with FRP laminates. Elastic model is applied for FRP laminate's behavior in the all reported researches.

Malek *et al.* (1998) has proposed an analysis method based on linear elastic behavior of the materials for calculating shear and normal stress concentration at the cutoff point of the plate.

Rasheed *et al.* (2004) developed an analytical solution for the load–deflection calculation of FRP strengthened simple beams at any load stage. The solution assumes a trilinear moment-curvature response characterized by the flexural crack initiation, steel yielding, and ultimate capacity. The first stage extends to the onset point of flexural cracking. The second one follows until the first yielding of the tension steel. The third line continues until the limit of concrete useful strain (0.003) or FRP rupture, depending on the flexural mode involved. Therefore, their analytical model was not considered the debonding of FRP. Reinforcing steel and concrete are assumed to have the classical linear elastic–perfectly plastic and elastic–plastic response respectively.

Chahrour and Soudki (2005) presented an inelastic section analysis to predict the mid-span moment-curvature response of strengthened beams with CFRP laminate. Bilinear and linear elastic-perfectly plastic model were used for concrete and steel behavior respectively. They did not apply any model for debonding of CFRP laminate in inelastic analysis. But, the analysis is based on the experimentally measured strains in CFRP laminate at the beam mid-span.

Toutanji *et al.* (2006) present an analytical model for the moment-deflection calculation of FRP strengthened simple beams at three points. First and second points are moment and deflection of cracking and yielding of steel at mid-span and third point is ultimate state. Debonding of FRP

laminate was considered in analytical model at ultimate state. Elastic–plastic and linear elastic-perfectly plastic were used concrete and steel behavior respectively.

Akbarzadeh and Maghsoudi (2010) developed an analytical model to predict moment-curvature, load capacity and the behavior of FRP strengthened continuous HSC beams. The stress-strain curves of concrete, steel and FRP were considered as integrity model. Stress–strain model of concrete was extended from Oztekin *et al.*'s model by modifying the ultimate strain. Also, debonding of FRP laminate was considered in analytical model.

Ebrahimpour and Maghsoudi (2013) presented a nonlinear analytical model to predict complete moment-curvature response, ultimate moment, ductility and failure mode of FRP strengthened RHSC beams. Collins *et al.* (1989) and bilinear elastic-plastic model were used for HSC and steel reinforcement behavior respectively. Also, premature debonding mode of FRP laminate was considered using ACI 440.2R-08 recommendations.

The new developments in concrete technology have led to increased applications of high-strength concrete, HSC, all around the globe. HSC offers many advantages over conventional concrete. When the strength of concrete gets higher, some of its characteristics and engineering properties become different from those of normal-strength concrete (NSC) (ACI 363R. 2010, Rashid *et al.* 2002, Maghsoudi and Akbarzadeh 2006). These differences in material properties may have important consequences in terms of the structural behavior and design of HSC members (Oztekin *et al.* 2003). High strength concrete, due to its very high compression strength, is less ductile; so in seismic areas, ductility is an important factor in design of HSC members (especially FRP strengthened structural members) under flexure.

In recent decades, soft computing approaches such as artificial neural networks (ANN), fuzzy inference systems (FIS), adaptive neuro-fuzzy inference systems (ANFIS) and genetic algorithms (GA) have been used successfully for modeling in civil engineering applications. Gu and Oyadiji (2008) applied ANFIS to control the environmentally induced vibration response of a multiple degree-of-freedom (MDOF) structure with MR damper. Cevik (2011) used soft computing techniques for modeling of strength enhancement of FRP confide concrete cylinders. Amani and Moeini (2012) used ANN and ANFIS to predict the shear strength of RC beams and compared results with building codes. Mashrei *et al.* (2013) applied the back-propagation neural network (BPNN) to predict the bond strength of FRP-to-concrete joints and compared results with existing analytical models. Mohammadhassani *et al.* (2013) employed ANFIS to predict deflection for high strength self-compacting concrete (HSSCC) deep beams.

In this study, ANFIS and multiple regression analysis are used to predict the curvature ductility factor of FRP strengthened RHSC beams. Also, the effects of concrete strength, steel reinforcement ratio, FRP stiffness and height to wide ratio of beam section on the flexural behavior and the curvature ductility factor of the FRP strengthened RHSC beams are evaluated using the analytical approach.

2. Prediction of curvature ductility factor

2.1 Methodology

For preparing the database, which used in ANFIS and multiple regression analysis, Ebrahimpour and Maghsoudi's (2013) analytical model has been applied. This analytical model (Fig. 1) uses the principles of strain compatibility and equilibrium, and the material constitutive

relations for the HSC, steel and FRP to predict flexural behavior. The assumptions include: i) linear strain distribution throughout the full depth of the section, ii) no slip between the longitudinal reinforcing steel and the surrounding concrete, iii) no slip between the externally bonded FRP sheets and concrete, iv) failure of the beam occurs when either the compressive strain in the concrete reaches ultimate strain (ε_{cu}) or the tensile strain in the FRP composites reaches its ultimate strain (ε_{fe}).

In order to predict debonding failure, based on ACI 440.2R (2008) recommendations, the effective strain of FRP laminates, ε_{fe}, is limited to the strain level at which debonding may occur, ε_{fd}, as defined by Eq. (1).

$$\varepsilon_{fd} = 0.41 \sqrt{\frac{f_c{}'}{nE_f t_f}} \leq 0.9\varepsilon_{fu} \qquad (1)$$

where n is number of plies, t_f is thickness for each ply (mm), E_f is tensile modulus of FRP (N/mm^2), $f_c{}'$ is the cylindrical compressive strength of concrete (N/mm^2), and ε_{fu} is design rupture strain of FRP laminates. Also the value of ε_{cu} is assumed to be equal to 0.0035 (CAN3-A23.3 1994).

The calculation procedures of moment-curvature relationship are follows: for any strain in the extreme compressive fiber of concrete ε_c, assume the neutral axis depth c, then the steel reinforcement strain ε_s' and ε_s, and the FRP strain ε_f, are determined from similar triangles of the strain diagram. The corresponding stresses f_c, f_{cs}, f_s and f_f developed in the concrete, compression and tension steel reinforcement and FRP laminate, respectively, and evaluated by using the respective stress-strain curves of materials. The compressive concrete force C_c, the compressive steel force C_{cs}, the tensile steel force T_s, and FRP force T_f, are calculated and the internal forces equilibrium condition is checked. If the equilibrium condition is satisfied, the internal bending moment (M) of the section can be obtained by taking the sum of the moments about the middle height of the section. Also, the corresponding curvature is calculated by dividing the concrete strain ε_c by a distance to the neutral axis depth, c

$$\phi = \frac{\varepsilon_c}{c} \qquad (2)$$

By carrying out repeated calculation of this procedure until ultimate state, the full-range moment-curvature response of a FRP strengthened RHSC beam section is obtained.

2.2 Parametric study

The ductility of a structural member may be defined as its ability to deform up to the failure load without a significant loss in its load-carrying capacity. In seismic areas, ductility is an important factor in design of RC members under flexure; Since FRP repair is newly innovation and also the HSC behavior is like a brittle material, therefore, understanding the effect of such materials on the ductility of the RC beams is critical (Maghsoudi and Akbarzadeh 2006). Ductility

factor can be calculated as defined by Eq. (3).

Table 1 Balanced reinforcement ratios for different HSC strengths

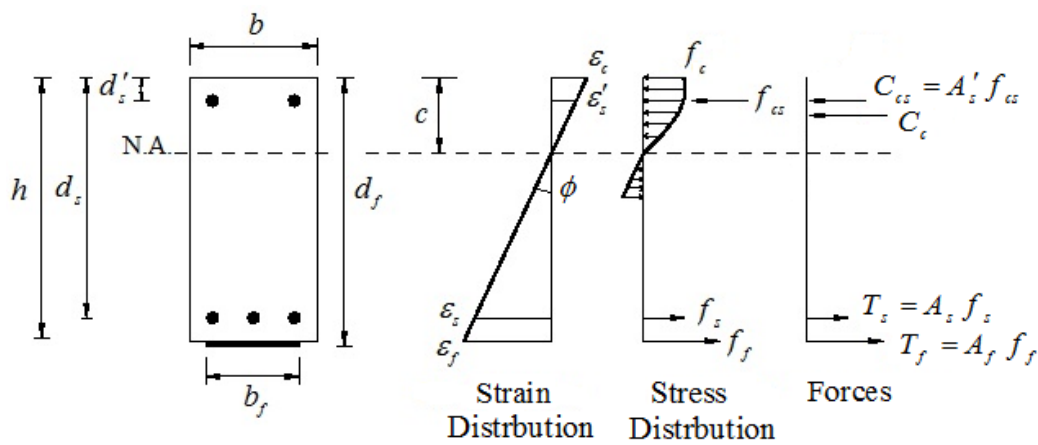| Type	Compressive strength of HSC, f_c' (MPa)				
	60	70	80	90	100
Balanced reinforcement ratio (ρ_b)	0.059	0.066	0.072	0.080	0.088

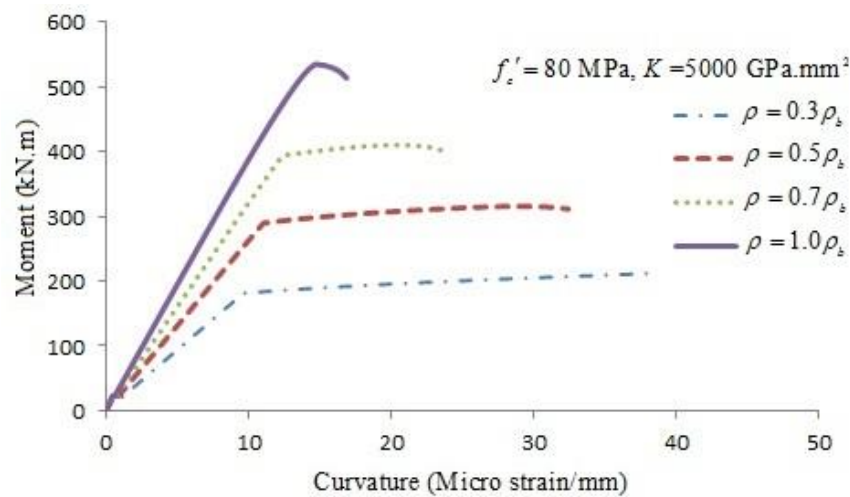Fig. 1 Strain, stresses and forces used in the moment–curvature model

Fig. 2 Analytical moment–curvature response for FRP strengthened RHSC beam sections with different steel ratio
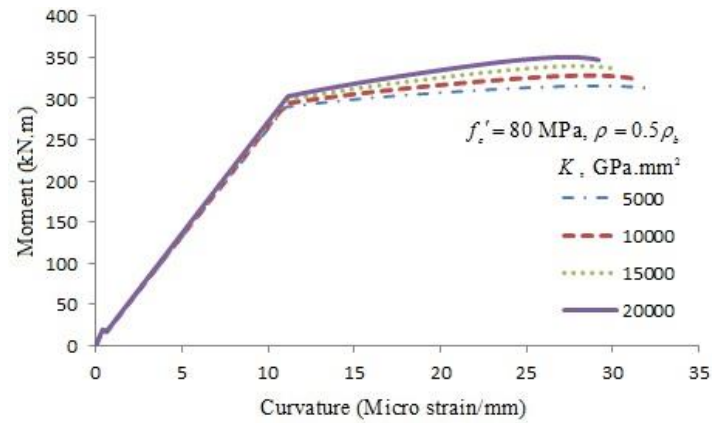
Fig. 3 Analytical moment–curvature response for FRP strengthened RHSC beam sections with different FRP stiffness
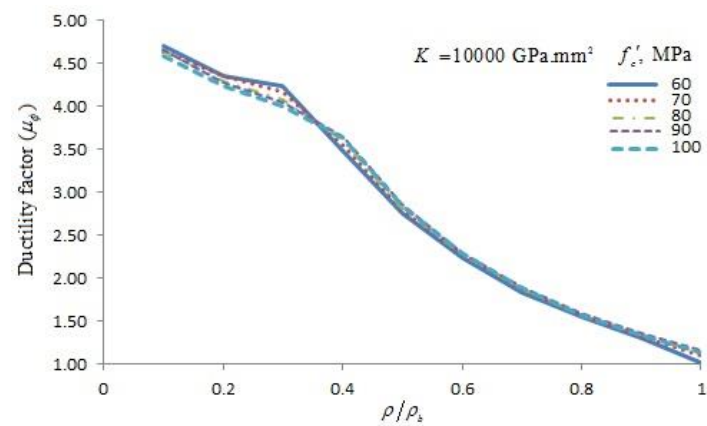

Fig. 4 Ductility factor of FRP strengthened RHSC beam sections against amount of steel reinforcement
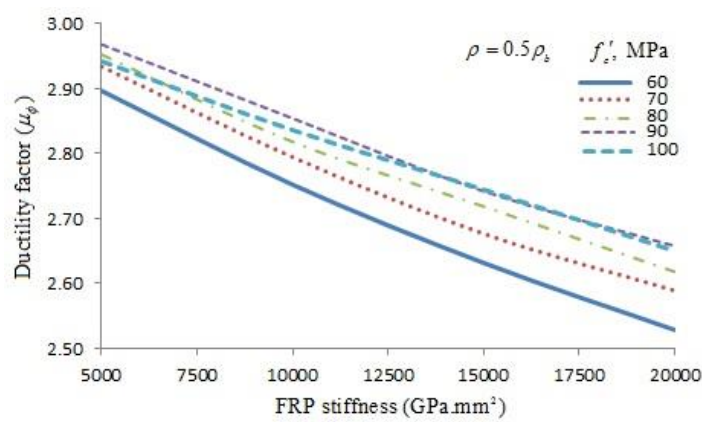

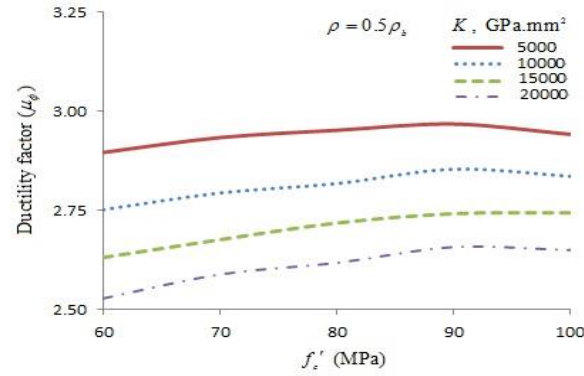Fig. 5 Ductility factor of FRP strengthened RHSC beam sections against FRP stiffness

Fig. 6 Ductility factor of FRP strengthened RHSC beam sections against HSC strength
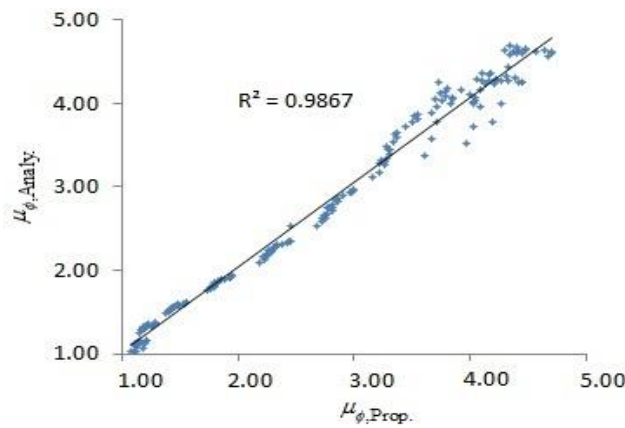

Fig. 7 Performance of MR model in predicting μ_ϕ

$$\mu_\phi = \frac{\phi_u}{\phi_y} \tag{3}$$

where ϕ_u is the curvature at beam ultimate load and ϕ_y is the curvature when the tension reinforcement first reaches the yielding strength.

In order to investigate the effects of concrete strength, steel reinforcement ratio and externally reinforcement (FRP) stiffness on the flexural behavior and the curvature ductility factor of the FRP strengthened RHSC beams; the rectangular type beam sections (Fig. 1.) are analytically simulated. A typical beam section has a width $b = 200$ mm, total depth $h = 400$ mm and the tension reinforcement is provided at depth $d = 340$ mm from the top. For parametric study, the cylindrical compressive strength of high strength concrete f'_c is varied from 60 to 100 MPa, the yield strength of reinforcing steel $f_y = 400$ MPa and Young's modulus of reinforcement steel $E_s = 200$ GPa.

The tension reinforcement ratio $\rho(\rho = A_s/bd)$ is varied from 10 to 100% of the balanced reinforcement ratio ρ_b of RHSC sections which are calculated by Eq. 4, and listed in Table 1.

$$\rho_b = \alpha\gamma\frac{f_c'}{f_y}(\frac{700}{700+f_y})$$ (4)

where α and γ are stress and centroid factors, respectively (more details can be found in Ebrahimpour and Maghsoudi (2013)).

Also the externally reinforcement (FRP) stiffness K ($K = E_f A_f$) is varied from 5000 to 20000 GPa.mm². FRP laminate's width and FRP rupture strain are assumed 200 mm and 1.5%, respectively.

The theoretical moment and curvature for FRP strengthened RHSC beams sections are calculated by the aforementioned analytical method. Fig. 2 shows some analytical moment-curvature responses of strengthened beam sections with concrete strength $f_c' = 80$ MPa, FRP stiffness $K = 5000$ GPa.mm² and different tension reinforcement ratio (ρ). Comparing theses curves for different steel ratio, it can be seen that the tension reinforcement ratio basically affects both the shape of moment-curvature curve and the ductility of a beam section; as increasing the tension reinforcement ratio, the plateau of curve at the post-peak stage becomes gradually shorter and drops more rapidly that indicating remarkable reduction in ductility.

Fig. 3 shows some selected moment-curvature responses of FRP strengthened RHSC beam sections with concrete strength $f_c' = 80$ MPa and tension reinforcement ratio $\rho = 0.5\rho_b$ for different FRP stiffness (K). The increase of FRP stiffness leads to increase of the failure moment and post-yield stiffness and also decrease the ultimate curvature but the curvature at yielding load remains almost constant

The curvature ductility factor μ_ϕ of FRP strengthened RHSC beam section is calculated by Eq. (3). Fig. 4 shows a plot of curvature ductility factor as a function of steel reinforcement ratio for FRP strengthened RHSC beam sections with FRP stiffness $K = 10000$ GPa.mm² and different HSC strengths. The curvature ductility factor decreases with increasing steel reinforcement ratio.

Fig. 5 shows a plot of curvature ductility factor as a function of FRP stiffness for FRP strengthened RHSC beam sections with steel reinforcement ratio $\rho = 0.5\rho_b$ and different HSC strengths. It indicates that the curvature ductility factor decreases with an increase in FRP stiffness.

Fig. 6 shows a plot of curvature ductility factor as a function of HSC strength for FRP strengthened RHSC beam sections with steel reinforcement ratio $\rho = 0.5\rho_b$ and different FRP stiffness. The curvature ductility factor increases with an increase in HSC strength, but up to a certain level of concrete strength, about 90 MPa; beyond this level, the curvature ductility factor slightly decreases as the HSC strength is increased.

2.3 Multiple regression (MR) model

According to the aforementioned analytical results, it is estimated that the HSC strength (f_c'), the amount of steel reinforcement (ρ/ρ_b), and FRP stiffness (K), have influence on the curvature ductility factor of FRP strengthened RHSC beam sections. Thus, the basic formation of the

curvature ductility factor equation for FRP strengthened RHSC beam sections can be expressed as defined by Eq. (5), by using multiple regression (MR) method.

$$\mu_\phi = f \left(f_c', \ \rho/\rho_b, \ K \right) \tag{5}$$

where f_c, ρ, ρ_b and K are the HSC strength, steel reinforcement ratio, balanced steel ratio of the beam section and FRP stiffness, respectively. Also based on the analytical results described previously, the curvature ductility factor and the amount of steel reinforcement, FRP stiffness and HSC strength are mutually related with the 2nd-order polynomial, 3rd-order polynomial and exponential function, respectively. So the prediction equation of the curvature ductility factor for FRP strengthened RHSC beam sections can be expressed as following

$$\mu_\phi = (a_1\{a_2(\rho/\rho_b)^3 + a_3(\rho/\rho_b)^2 + a_4(\rho/\rho_b) + a_5\} \\ \times (K)^{a_6} \times \{a_7(f_c')^2 + a_8(f_c') + a_9\}) \tag{6}$$

where the coefficient a_i are determined from MR analysis, which is using the analytical results (Lee 2013). In Sec. 2.4, one can find more details about training and testing data which used in MR technique. By carrying out the MR method, the following equation is suggested for the prediction of curvature ductility factor of FRP strengthened RHSC beams, based on the parametric study

$$\mu_\phi = (\{7.698(\rho/\rho_b)^3 - 11.564(\rho/\rho_b)^2 + 0.466(\rho/\rho_b) + 4.572\} \\ \times (K)^{-0.057} \times \{-8.0 \times 10^{-5}(f_c')^2 + 0.014(f_c') + 1.087\}) \tag{7}$$

Fig. 7 shows the comparison of the proposed curvature ductility factor obtained by Eq. (7) with the analytical results. The MR model's predictions show excellent agreement as evident from coefficients correlation R^2 well above 98.67% and the mean error is 1.87%, so it means that the proposed equation is accurate enough for practical applications.

2.4 ANFIS model

Fuzzy systems can be connected with artificial neural networks to form neuro-fuzzy systems, as combination of the natural language description of fuzzy systems and the learning properties of neural networks, which exhibit advantages of both soft computing approaches. The adaptive neuro-fuzzy inference system (ANFIS), which developed by Jang *et al.* (1997) is one of the modeling systems which allows the fuzzy systems to learn the parameters using adaptive back-propagation learning algorithm. ANFIS models consists of three distinct segments: i) the input parameters and membership functions, ii) the adaptive neuro-fuzzy inferencing system, iii) the output parameter and the defuzzifier, if necessary. A schematic view of an ANFIS object is shown in Fig. 8.

Mamdani and Sugeno fuzzy models are the mainly types of fuzzy inference systems, which have been widely employed in various applications. The differences between these fuzzy inference systems (FIS) are due to the consequents of their fuzzy rules, and thus their aggregation and defuzzification procedures differ accordingly (Jang *et al.* 1997). In this study the Sugeno FIS is used where each rule is defined as a linear combination of input variables. The corresponding final output of the fuzzy model is simply the weighted average of each rule's output. A Sugeno FIS

consisting of two input variables x and y, for example, a one output variable f will lead to two fuzzy rules:

Rule 1: If x is A_1, y is B_1 then $f_1 = p_1x + q_1y + r_1$

Rule 2: If x is A_2, y is B_2 then $f_2 = p_2x + q_2y + r_2$

where p_i, q_i, and r_i are the consequent parameters of i-th rule. A_i, B_i and C_i are the linguistic labels which are represented by fuzzy sets shown in Fig. 9.

Table 2. Properties of database

Property		f_c' (MPa)	K (GPa.mm^2)	ρ/ρ_b
Mean Value	Train	81.08	12269.23	0.56
	Test	78	12928.57	0.53

Table 3. Comparison of errors in proposed models

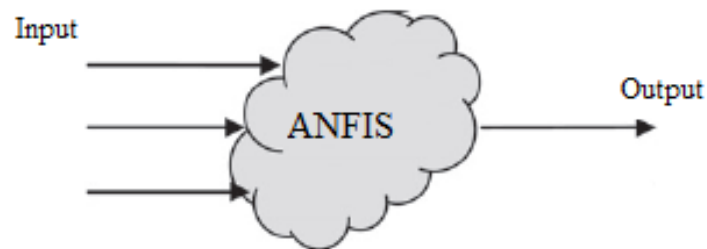| Method	RMSE (%)	R^2	Mean Error (%)
Multiple Regression (MR)	14.98	0.9867	1.87
ANFIS	4.64	0.9986	-0.22

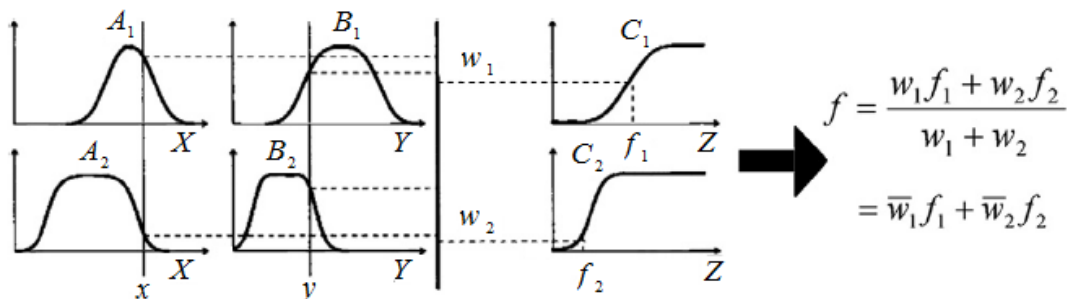Fig. 8 Schematic view of ANFIS

Fig. 9 The Sugeno fuzzy model (Jang *et al.* 1997)
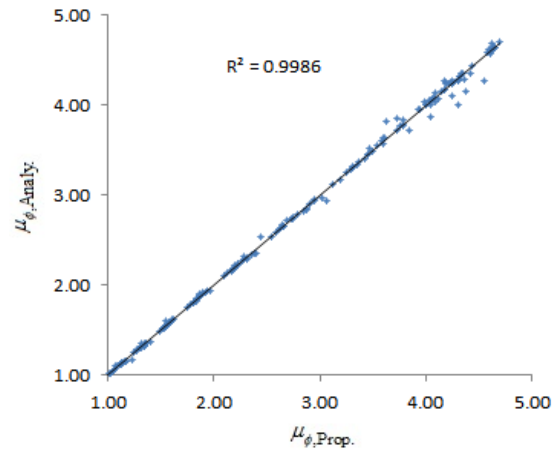
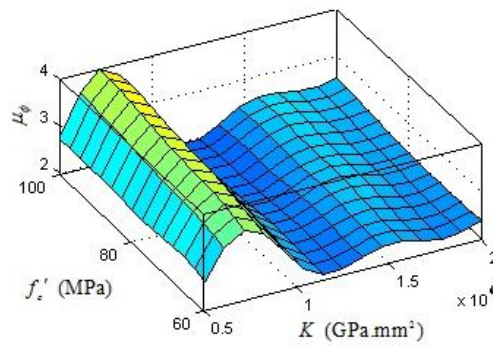Fig. 10 Performance of ANFIS model in predicting μ_ϕ

Fig. 11 Fuzzy surface: HSC Strength and FRP stiffness versus μ_ϕ prediction
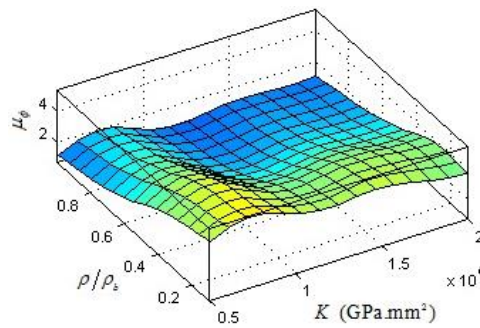

Fig. 12 Fuzzy surface: Steel reinforcement ratio and FRP stiffness versus μ_ϕ prediction
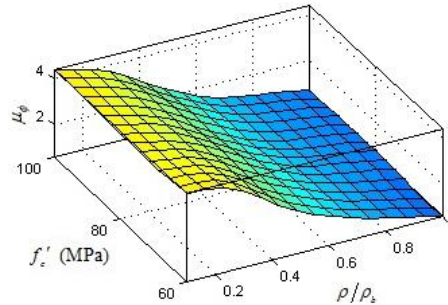
Fig. 13 Fuzzy surface: HSC Strength and Steel reinforcement ratio versus μ_ϕ prediction

The present implementation of ANFIS model was carried out using the fuzzy logic toolbox available in MATLAB software. The implementation permits choosing the number and type of membership function associated with each input and the number of epochs required for training the ANFIS. The generation of the network and tuning of the network parameters to match the expected target values are fully automated, with provision for supplying a test data set along with the training set to avoid over-fitting the inference system. The input parameters supplied to ANFIS model are the HSC strength, steel reinforcement ratio and FRP stiffness, based on parametric study.

The choice of membership functions was made by conducting a trial run of the ANFIS objects generated using several alternative functions like triangular membership function, trapezoidal membership function, sigmoid membership function, generalized bell membership function, Gaussian membership function, S-Shaped membership function. The present data showed minimum error levels for Gaussian input membership function. The output membership function can either be a constant membership function or a linear membership function. For the present data, constant output membership function produced the minimum error. In this study, 70% of the data sets are randomly chosen as training data and the remains 30% as testing data. The properties of parameters in these data-sets are given in Table 2.

Fig. 10 shows the comparison of the proposed ANFIS model with the analytical results, which reveals that the proposed ANFIS method is highly accurate by coefficients correlation R^2 of above 99.86% and the mean error of -0.22%. The relation between input variables and curvature ductility output variable can be visualized with the modeled fuzzy surfaces shown in Figs. 11-13.

The comparison of the root mean squared errors (RMSE), R^2 and mean errors between ANFIS and MR models are presented in Table 3. RMSE were calculated as the root mean squared error for the parameter divided by the mean of the parametric values and converted to percentage.

The comparison of results indicated that ANFIS model's RMSE is approximately 3 times smaller than MR model's value. In addition, the ANFIS model modified the less agreement which observed for high curvature ductility factors in MR model (see Figs. 7 and 10). These errors, which made by using less accurate function for the case of lower steel reinforcement ratio in MR model, could be omitted by using the adaptive neuro-fuzzy inference algorithm in ANFIS model. However by considering the overall results, one can find that both proposed models are suitable for practical applications.

2.5 Modified formula based on dimensional effect

To extend application of proposed models based on dimensional effect, the parametric study which considered height to wide ratio (h/b) of beam section's effect is conducted. Three considered values of this ratio are 1.0, 1.5 and 2.0 (mm/mm).

Figs. 14 and 15 show the comparison between the proposed models and the analytical results with respect to (h/b) ratio. The MR and ANFIS models' predictions show good agreements as evident from coefficients correlation R^2 well above 92.01%, 96.67% and 98.67%, and 97.79%, 99.66% and 99.86% for (h/b) ratios equal to 1.0, 1.5 and 2.0 (mm/mm), respectively.

Based on obtained results, one could express the modified formula for curvature ductility factor of FRP strengthened RHSC beam sections as follow

$$\mu_\phi = \lambda . \mu_{\phi,\text{Prop.}} \tag{8}$$

where λ and $\mu_{\phi,\text{Prop.}}$ are coefficient which depends on dimensional effect and curvature ductility factor based on proposed models, respectively. The calibration of the results obtained allows estimating the coefficient λ as presented in Table 4.

Table 4 Estimate of the coefficient λ based on dimensional effect

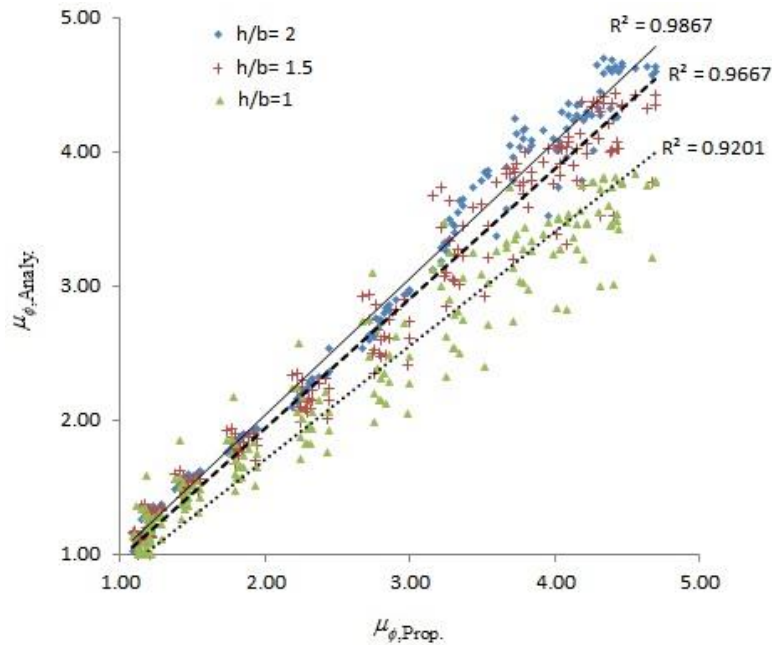| Coefficient		h/b (mm/mm)		
		1.0	1.5	2.0
λ	MR model	1.0187	0.9650	0.8483
	ANFIS model	0.9978	0.9466	0.8256

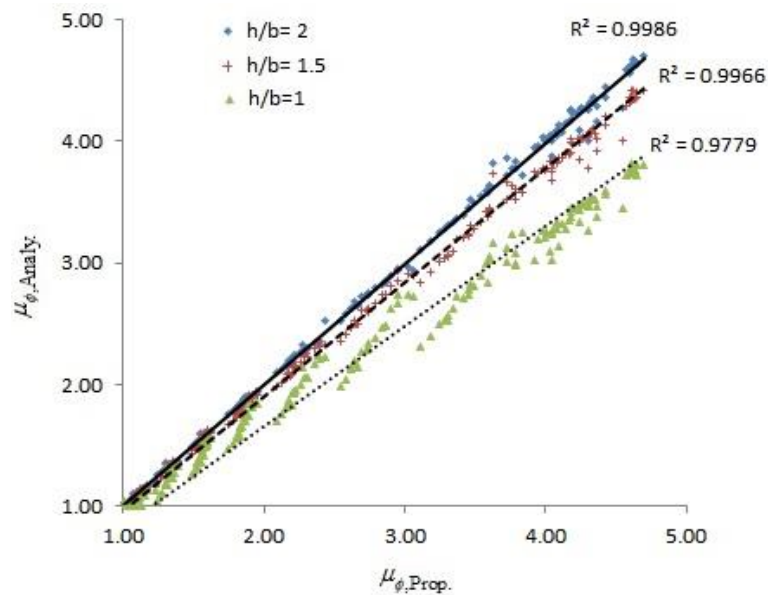Fig. 14 Performance of MR model in predicting μ_ϕ with respect to dimensional effect

Fig. 15 Performance of ANFIS model in predicting μ_ϕ with respect to dimensional effect

3. Conclusions

In this study, the applications of the Adaptive Neuro-Fuzzy Inference System (ANFIS) and Multiple Regression (MR) methods for prediction of the curvature ductility factor of FRP strengthened reinforced HSC (RHSC) beams have been demonstrated. The effects of HSC strength, steel reinforcement ratio and FRP stiffness on flexural behavior and curvature ductility factor of FRP strengthened RHSC beam sections have been studied and newly MR and ANFIS prediction models for curvature ductility factor have been developed. Also, the modified formula based on dimensional effect is presented.

The curvature ductility factor of FRP strengthened RHSC beam sections increases with an increase in HSC strength, but up to a certain level of concrete strength about 90 MPa and decreases with an increase of steel reinforcement ratio and FRP stiffness, respectively.

Results indicate that the predictions of ANFIS and MR models for the curvature ductility factor are accurate to within -0.22% and 1.87% error for practical applications respectively.

References

ACI 363R. (2010), *State-of-the-art report on high-strength concrete*, American Concrete Institute, Detroit.
ACI 440.2R. (2008), *Guide for the design and construction of externally bonded FRP systems for strengthening concrete structures*, American Concrete Institute, Farmington Hills, Michigan.
Akbarzadeh, H. and Maghsoudi, A.A. (2010), "Experimental and analytical investigation of reinforced high strength concrete continuous beams strengthened with fiber reinforced polymer", *Mater. Design.*, **31**(3), 1130-1147.
Amini, J. and Moeini, R. (2012), "Prediction of shear strength of reinforced concrete beams using adaptive

neuro-fuzzy inference system and artificial neural network", *Sci. Iran. Trans. A.*, **19**(2), 242-248.

CAN3-A23.3 (1994), *Design of Concrete Structure for Buildings (CAN3-A23.3-M94)*, Canadian Standards Association (CSA), Rexdale, Ontario.

Cevik, A. (2011), "Modeling strength enhancement of FRP confined concrete cylinders using soft computing", *Expert. Syst. Appl.*, **38**(5), 5662-5673.

Chahrour, A. and Soudki, K. (2005), "Flexural response of reinforced concrete beams strengthened with end-anchored partially bonded carbon fiber-reinforced polymer strips", *J. Compos. Construct.*, **9**(2), 170-177.

Collins, M.P. and Porasz, A. (1989), "Shear design for high-strength concrete", *Comité Euro-International du Béton, Bulletin d'Information*, **193**, 77-83.

Ebrahimpour Komleh, H. and Maghsoudi, A.A. (2013), "Analytical Investigation on Ductility of CFRP/GFRP Strengthened RHSC Beams", *Proceedings of the 4th International Conference on Concrete and Development*, Tehran, Iran, April.

Foret, G. and Limam, O. (2008), "Experimental and numerical analysis of RC two-way slabs strengthened with NSM CFRP rods", *Constr. Build. Mater.*, **22**(10), 2025-2030.

Gu, Z.Q. and Oyadiji, S.O. (2008), "Application of MR damper in structural control using ANFIS method", *Comput. Struct.*, **86**(3-5), 427-436.

Hashemi, S.H., Maghsoudi, A.A, and Rahgozar, R. (2009), "Bending response of HSRC beams strengthened with FRP sheets", *Sci. Iran. Trans. A.*, **16**(2), 138-146.

Jang, J.S.R., Sun, C.T., and Mizutani, E. (1997), *Neuro-fuzzy and soft computing.Computational approach to learning and machine intelligence*, Prentice Hall.

Lee, H.J. (2013), "Predictions of curvature ductility factor of doubly reinforced concrete beams with high strength materials", *Comput. Concrete.*, **12** (6), 831-850.

Lignola, G.P., Prota, A., Manfredi, G. and Gosenza, E. (2007), "Experimental performance of RC hollow columns confined with CFRP", *J. Compos. Constr.*, **11**(1), 42-49.

Maghsoudi, A.A. and Akbarzadeh, H. (2006), "Flexural ductility of HSC members", *Struct. Eng. Mech.*, **24**(2), 195-212.

Malek, A.M., Saadatmanesh, H. and Ehsani, M.R. (1998), "Prediction of failure load of R/C beams strengthened with FRP plate due to stress concentration at the plate end", *ACI. Struct. J.*, **95**(2), 142-152.

Mashrei, M.A., Seracino, R. and Rahman, M.S. (2013), "Application of artificial neural networks to predict the bond strength of FRP-to-concrete joints", *Constr. Build. Mater.*, **40**, 812-821.

Mohammadhassani, M., Nezamabadi-Pour, H., Jumaat, M., Jameel, M., Hakim, S.J.S. and Zargar, M. (2013), "Application of the ANFIS model in deflection prediction of concrete deep beam", *Struct. Eng. Mech.*,**45**(3), 319-332.

Oehlers, D.J. (2001), "Development of design rules for retrofitting by adhesive bonding or bolting either FRP or steel plates to RC beams or slabs in bridges and building", *Compos. Part. A. - Appl. S.,* **32**(9), 1345-1355.

Oztekin, E., Pul, S. and Husem, M. (2003), "Determination of rectangular stress block parameters for high performance concrete", *Eng. Struct.*, **25**(3), 371-376.

Park. R. and Paulay, T. (1975), *Reinforced Concrete Structure*, John Wiley and Sons, New York, USA.

Rasheed, H.A., Charkas, H. and Melhem, H. (2004), "Simplified nonlinear analysis of strengthened concrete beams based on a rigorous approach", *J. Struct. Eng.*, **130**(7), 1087-1096.

Rashid, M.A., Mansur, M.A. and Paramasivam, P. (2002), "Correlations between mechanical properties of high-strength concrete", *J. Mater. Civil. Eng.*, **14**(3), 230-238.

Rashid, M.A. and Mansur, M.A. (2005), "Reinforced high-strength concrete beams in flexure", *ACI. Struct. J.*, **102**(3), 462-471.

Teng, J.G., Chen, J.F., Smith, S.T. and Lam, L. (2002), *FRP strengthened RC structures*, Wiley, New York, USA.

Toutanji, H., Zhao, L. and Zhang, Y. (2006), "Flexural behavior of reinforced concrete beams externally strengthened with CFRP sheets bonded with an inorganic matrix", *Eng. Struct.*, **28**(4), 557-566.

Xiong, G.J., Yang, J.Z. and Ji, Z.B. (2004), "Behavior of reinforced concrete beams strengthened with externally bonded hybrid carbon fiber-glass fiber sheets", *J. Compos. Constr.*, 275-278.

CC